Carrier recombination rates in narrow-gap InAs/$Ga_{1-x}In_xSb$-based superlattices

Michael E. Flatté
Department of Physics and Astronomy, University of Iowa, Iowa City, Iowa 52242
and Optical Science and Technology Center, University of Iowa, Iowa City, Iowa 52242

C. H. Grein
Department of Physics, University of Illinois, Chicago, Illinois 60607

T. C. Hasenberg
Department of Physics and Astronomy, University of Iowa, Iowa City, Iowa 52242
and Optical Science and Technology Center, University of Iowa, Iowa City, Iowa 52242

S. A. Anson
Department of Electrical and Computer Engineering, University of Iowa, Iowa City, Iowa 52242
and Optical Science and Technology Center, University of Iowa, Iowa City, Iowa 52242

D.-J. Jang and J. T. Olesberg
Department of Physics and Astronomy, University of Iowa, Iowa City, Iowa 52242
and Optical Science and Technology Center, University of Iowa, Iowa City, Iowa 52242

Thomas F. Boggess
Department of Physics and Astronomy, University of Iowa, Iowa City, Iowa 52242;
Optical Science and Technology Center, University of Iowa, Iowa City, Iowa 52242;
and Department of Electrical and Computer Engineering, University of Iowa, Iowa City, Iowa 52242
(Received 6 October 1997; revised manuscript received 4 June 1998)

We present a comparison of theoretical calculations and experimental measurements of the Auger recombination rate in a narrow-gap semiconductor superlattice with a complex band structure. The calculations and measurements indicate that the rate depends on density as n^2 for low density, and changes to an n dependence when the electrons and holes become degenerate. The calculations are the first to incorporate superlattice umklapp processes, which contribute about half of the total rate and substantially improve the agreement with experiment. [S0163-1829(99)04203-4]

I. INTRODUCTION

One of the most challenging electronic properties to calculate properly in a semiconductor is the carrier lifetime due to nonradiative processes in a dense electron-hole plasma. In the nonradiative processes of interest, direct Auger processes, an electron-hole pair recombines and the excess energy and momentum is transferred to another carrier. Direct Auger processes will typically dominate over radiative processes and phonon-assisted or impurity-assisted Auger processes in high-quality direct-gap semiconductors at 300 K with (roughly) band gaps less than 0.5 eV and electron-hole pair densities greater than 10^{17} cm^{-3}. Since states at large momentum and large excess energy are involved in direct Auger processes, the recombination rate can be extremely sensitive to delicate features of the electronic structure. Hence accurate calculations of the Auger rates require accurate calculations of the nonparabolic band structures and the matrix elements between states of very different momentum in the same band or in different bands. For example, analytic expressions based on parabolic bands and nonparabolic bands in InSb differ[1] by a factor of 4.

A disparity of an order of magnitude is common between calculated and measured Auger rates in direct-gap bulk semiconductors. In InSb, the rates calculated using nonparabolic bands, matrix elements calculated from the Kane model, and static screening[2] are a factor of 7 smaller than the experimentally observed values.[3] In InAs, however, experimental rates[4] were within 15% of those estimated for a parabolic band model without screening.[5] In $In_{0.53}Ga_{0.47}As$ theoretical estimates[6] were an order of magnitude *higher* than experimental rates.[7] These calculations and measurements are typically performed in the nondegenerate density regime, especially for the valence band. It is likely that the difficulty of calculating Auger rates in bulk semiconductors, despite their straightforward band structures, is related to the substantially greater band-edge density of states in the valence band relative to the conduction band, and the heavy-hole–light-hole degeneracy.

Strained semiconductor superlattices, however, do not have these complications. Strain not only removes the heavy-hole–light-hole degeneracy, but it makes the top valence subband's in-plane mass light, lessening the density of states mismatch between valence and conduction bands. Despite the possibility of more accurate calculations in heterostructures, and the ability to excite degenerate electron-hole plas-

mas optically at lower densities than in bulk semiconductors, calculations of Auger rates for semiconductor heterostructures are quite rare. Results for infinite-barrier quantum wells[8] were never compared with experiment. The only detailed comparison of theory with experiment[9] concerned an extremely narrow-gap (0.113 eV at 300 K) $InAs/In_{0.25}Ga_{0.75}Sb$ superlattice grown on GaSb. The biaxially compressive strain in the $In_{0.25}Ga_{0.75}Sb$ layer, combined with confinement energy, is sufficient to split the top heavy-hole subband from the next valence subband by 0.245 eV, an amount substantially greater than the energy gap. Momentum and energy conservation within this band structure combine to suppress the Auger rate[10,11] strongly, as confirmed by experiment.[9] The experimental results of Ref. 9, however, did not explore the detailed density and temperature dependence of the Auger rate. Additionally, the unusually simple ''three-band'' electronic structure of this superlattice causes the Auger rate to depend in a more limited way on the accuracy of details of the band structure.

In addition to measurements of Auger rates based on photoconductivity measurements, Auger rates as a function of temperature have been extracted from laser device performance.[12] This technique, however, requires assumptions concerning the density dependence of the Auger rate (typically that the rate per carrier is proportional to n^2), and provides information on the rate at a different density for each temperature. Thus the temperature and density dependence of the Auger rate cannot be properly disentangled.

In this work we consider a more rigorous test case for Auger calculations in heterostructures. By considering a heterostructure with a complex band structure, we require our calculations of the energies and matrix elements among states to be exceptionally accurate. We compare with measurements of the density dependence of the Auger rate at 300 K and the temperature dependence of the rate at a fixed density. Our calculation captures not only the density and temperature dependence of the rate, but also its absolute magnitude well within the experimental and theoretical errors. The agreement in absolute magnitude would be impossible if superlattice umklapp processes were not included, for they account for about half of the total Auger rate. In contrast, in *bulk* narrow-gap semiconductors, which have larger reciprocal-lattice vectors, the umklapp processes are insignificant.[13] We conclude that for this superlattice a detailed understanding of the single-particle band structure and matrix elements is of paramount importance, and simple models of the Auger processes fail.

II. SAMPLE STRUCTURE

Our structure consists of 40 periods of a narrow-gap (0.31 eV at 300 K) type-II four-layer superlattice[14] with unit cells of 15-Å InAs, 25-Å $In_{0.40}Ga_{0.60}Sb$, 15-Å InAs, and 39-Å $Al_{0.30}In_{0.28}Ga_{0.42}As_{0.50}Sb_{0.50}$ grown on a GaSb substrate, not intentionally doped, and with a 50-Å GaSb cap. Auger transitions are possible for final states at least one energy gap (E_g) above the conduction minimum or E_g below the valence maximum. These ''resonance'' energies (shown in Fig. 1) occur within the band-edge extremes of the bulk constituents of the superlattice, and hence lie in regions of the band structure which have pronounced spectral features. Figure 2

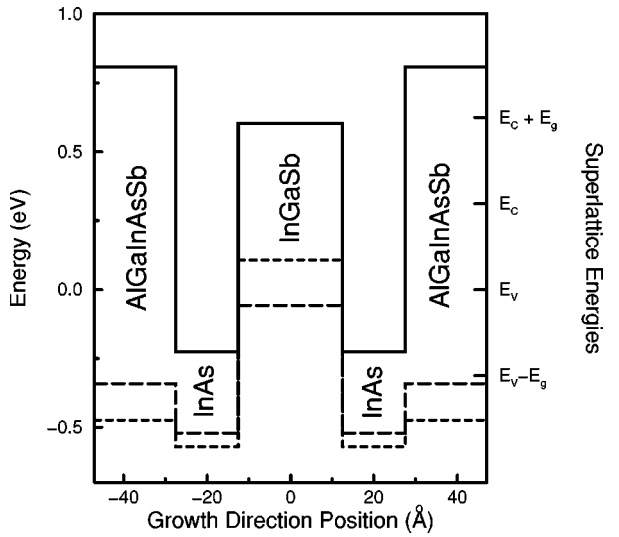

FIG. 1. Conduction (solid), heavy-hole (short dashed), and light-hole (long dashed) band-edge energies for the constituents of the four-layer superlattice. Conduction- (E_C) and valence- (E_V) band edges for the four-layer superlattice are shown on the right edge of the figure, as are the resonance energies for Auger processes ($E_C + E_g$ and $E_V - E_g$).

shows the growth-direction band structure and the projection onto a line plot of the two-dimensional band structure parallel to the interfaces. Dashed lines indicate the band edges and resonance energies. The superlattice layer thicknesses have been chosen to eliminate states with zero in-plane momentum in resonance regions. This type of band structure is quite

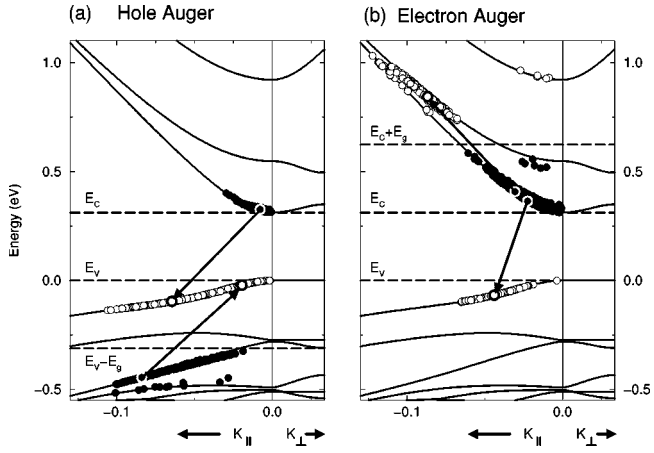

FIG. 2. Band structure of the superlattice indicating the band edges and the resonance energies (dashed lines) as well as the most probable transitions (99%) at 300 K and $n = 5 \times 10^{17}$ cm^{-3} for (a) hole Auger and (b) electron Auger processes, plotted as a function of *in-plane* momentum only. The single most probable transition is shown (with arrows) as a schematic Auger process with holes indicated by the larger, dark empty circles, and electrons indicated by filled circles. Since a slice of the three-dimensional band structure is shown, momentum-transfer vectors are projected onto the slice and the schematic scattering process appears not to conserve momentum. This is a result of projecting the three-dimensional band structure onto a line plot. $K_\perp$ is the momentum along the growth direction, while $K_\parallel$ is the momentum parallel to the interfaces.

different from that of a GaAs/$Al_yGa_{1-y}As$ quantum-well system, where the final states for an Auger event lie in regions of the band structure which are not highly structured and in fact are quasicontinuous. Due to the highly structured nature of the band structure near the resonance energies in the four-layer superlattice, the calculated Auger rate should be extremely sensitive to errors in the calculated band structure.

III. AUGER CALCULATIONS

The Auger processes involve two initial nonequilibrium carriers and two final states. Schematic hole and electron processes are shown in Figs. 2(a) and 2(b), respectively (indicated by their in-plane momentum only); these processes are the most probable for this band structure at $n=5\times10^{17}$ cm^{-3}. Most of the transitions involve nonequilibrium electrons and holes which have substantial in-plane momentum (and thus substantial excess energy relative to the band edge), and so are not highly occupied. Final states in the third valence subband dominate the hole Auger rate, while final states in the second conduction subband dominate the electron Auger rate. Golden rule calculations are performed with the full nonparabolic band structure and momentum-dependent matrix elements obtained from a superlattice $\mathbf{K}\cdot\mathbf{p}$ formalism similar to Ref. 15, but generalized to an arbitrary number of layers in a superlattice unit cell. Input parameters (tabulated for this system in Ref. 16) to the calculation are limited to energy levels, matrix elements, effective masses of bulk constituents, and valence-band offsets between layers. Changes in temperature are assumed to have important effects only on the band gaps of the bulk constituents. Transition matrix elements are evaluated using a statically screened Coulomb interaction and first-order $\mathbf{K}\cdot\mathbf{p}$ perturbation theory for the wave-function overlaps. Details of the formalism, not including umklapp, are available in Ref. 11. This superlattice $\mathbf{K}\cdot\mathbf{p}$ formalism has been successful in calculating the optical properties of related type-II multilayer structures.[17]

New to the calculation, to our knowledge, are umklapp processes in the superlattice growth-axis direction which contribute approximately half of the total Auger rate for this superlattice. Umklapp processes involve the additional transfer of a reciprocal-lattice vector $\mathbf{G}$ in the scattering process, and can be associated with scattering of the electrons and holes from the periodic potential of the superlattice. Thus they are properly considered *intrinsic* to the superlattice—they are present in perfectly clean samples. Umklapp processes in bulk semiconductors are known to be unimportant for Auger processes,[13] but, due to the large unit-cell size of the superlattice and the correspondingly small magnitude of the reciprocal-lattice vectors associated with the superlattice period, those conclusions cannot be extended to superlattices.

Formally, addition of umklapp processes changes the Auger rate R per unit volume for processes involving two nonequilibrium holes in the highest hole subband, a nonequilibrium electron in the lowest conduction subband, and a final state in a light-hole band from that written in Eq. (3.7) of Ref. 11 to

$$R=\frac{3e^4\hbar^3}{8\pi^6\epsilon^2m^4}(1-e^{-(\mu_e-\mu_h)/kT})\sum_{\mathbf{G}}\int\int\int d^3\mathbf{K}_1d^3\mathbf{K}_2d^3\mathbf{K}_{2'}f_p(\mathbf{K}_1)f_p(\mathbf{K}_2)f_n(\mathbf{K}_1+\mathbf{K}_2-\mathbf{K}_{2'})$$
$$\times\frac{\beta_{HH,C}(\mathbf{K}_1,\mathbf{K}_1+\mathbf{K}_2-\mathbf{K}_{2'}+\mathbf{G})\beta_{HH,LH}(\mathbf{K}_2,\mathbf{K}_{2'}-\mathbf{G})}{[\lambda^2+|\mathbf{K}_{2'}-\mathbf{K}_2-\mathbf{G}|^2]^2}$$
$$\times\delta[E_C(\mathbf{K}_1+\mathbf{K}_2-\mathbf{K}_{2'})+E_{LH}(\mathbf{K}_{2'})-E_{HH}(\mathbf{K}_1)-E_{HH}(\mathbf{K}_2)]. \quad (1)$$

Here $\beta_{L,L'}(\mathbf{K},\mathbf{K}')$ is the wave-function overlap of superlattice states L and L' with superlattice momenta $\mathbf{K}$ and $\mathbf{K}'$, $E_L(\mathbf{K})$ is the dispersion relation of the Lth superlattice state, and f_n and f_p are electron and hole Fermi functions, respectively, with the corresponding quasichemical potentials μ_e and μ_h. λ is the reciprocal screening length, e is the electron charge, $\hbar$ is Planck's constant, m is the electron's free mass, ϵ is the dielectric constant, and T is the temperature. The essential change in the formalism is the addition of the sum over $\mathbf{G}$ and the appearance of $\mathbf{G}$ in the screened Coulomb potential and the wave-function overlaps. Expressions for transitions among other states can be straightforwardly extended from Ref. 11. For the 4.0-μm superlattice, processes involving a reciprocal-lattice vector larger than $5(2\pi/D)$, where D is the superlattice period, are negligible.

As a preliminary test we have redone calculations for an 8.8-μm superlattice at 77 K (Ref. 9). The Auger rate for this system, a 39-Å InAs/25-Å $Ga_{0.75}In_{0.25}Sb$ superlattice, was determined from photoconductivity measurements. The old calculations, which did not include umklapp, and our calculations, which do, are shown in Fig. 3 along with the experimental values. The increase of a factor of 2 in the Auger rate significantly improves the correspondence between theory and experiment. Now the disagreement is on the order of 25%. We note that there is substantial uncertainty in the measured value of the Shockley-Read-Hall (SRH) lifetime for this sample using this method. Alternative choices for the SRH lifetime within the error bars of the measurement would improve the fit at the low-density end.

IV. OPTICAL MEASUREMENTS

Measurements of the carrier recombination rate in the 4.0-μm band-gap superlattice were performed using time-

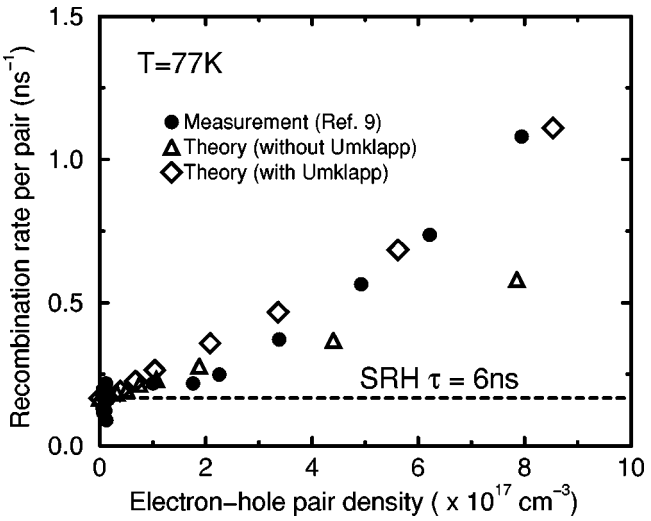

FIG. 3. Theoretical and experimental recombination rate as a function of the electron-hole pair density for a 8.8-μm system measured at 77 K in Ref. 9. The filled circles are the experimental points, and the triangles are the calculations reported in Ref. 9, which do not include umklapp processes. The diamonds are calculations which do include umklapp processes.

resolved differential transmission[18] and time-resolved photoluminescence (PL) upconversion.[19,20] Pulses of 140-fs duration and photon energy 1.476 eV from a mode-locked Ti:sapphire laser were used to excite electron-hole pairs in the superlattice. For the differential transmission measurements 170-fs probe pulses from a synchronously pumped optical parametric oscillator were used to probe the transmission at 0.349 eV. The time-resolved $\Delta T/T$ is shown in Fig. 4(a) for several values of the pump power. For the PL upconversion measurements, a delayed piece of the pump pulse (gating pulse) was mixed with the midinfrared PL in a nonlinear crystal, and the upconverted light intensity was detected [shown in Fig. 4(b) for a lattice temperature of 150 K and a photon energy corresponding to the peak of the PL spectrum]. For both methods the signal increases as the initially hot carriers relax to the band-edge states, and then decays as the carriers recombine.

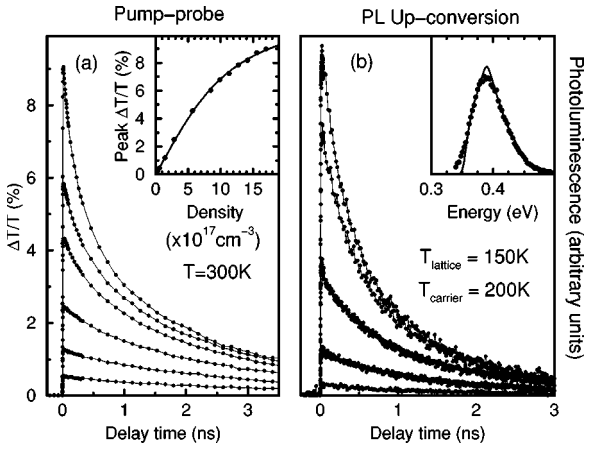

FIG. 4. (a) Differential transmission ($\Delta T/T$) vs pump-probe delay in the 4.0-μm sample for several initial excitation densities. The inset shows the relationship between the maximum $\Delta T/T$ and the density, measured (filled circles) and calculated (scaled vertically to agree with the measurements and indicated by the solid line). (b) PL upconverted intensity vs time from pump. The inset shows a comparison of the experimental (filled circles) and theoretical (solid line) PL spectra 10 ps after excitation to a density of 5.5×10^{17} cm^{-3}.

For the pump-probe measurements the initial carrier density is estimated from the dependence of the maximum $\Delta T/T$ on pump power, compared to its theoretical dependence on electron-hole density, both shown in the inset of Fig. 4(a). An independent estimate is obtained from the time-resolved photoluminescence spectrum at 10 ps, shown in the inset of Fig. 4(b) along with a theoretical calculation. We assume the carriers diffuse to a nearly uniform distribution along the growth direction of the sample on a time scale short compared to the recombination time. Our estimates of the excitation density with these methods are consistent with the number of photons in the pump pulse.

We express the recombination rate per electron-hole pair as

$$R(n)=\frac{1}{n}\frac{dn}{dt}=\frac{1}{n}\frac{dn}{dS}\frac{dS}{dt}, \tag{2}$$

where S is either the differential transmission (pump probe) or the PL intensity (PL upconversion). The two derivatives in Eq. (2) are readily related to the data of Fig. 4, allowing us to obtain an experimentally determined recombination rate as a function of density and temperature.

V. COMPARISON OF THEORY AND EXPERIMENT

Figure 5(a) shows these rates as a function of carrier density from the pump-probe measurements at 300 K. The zero-density intercept of the data is the (impurity-assisted) SRH recombination rate (0.37 ns^{-1}), and deviations from zero slope are associated with Auger recombination. Despite the large number of interfaces and the incorporation of a quinternary alloy in this superlattice, the structure is of high quality as indicated by the low SRH rate. We note that the theoretical radiative rate never exceeds 0.05 ns^{-1} for the carrier densities of interest, and is therefore insignificant relative to the nonradiative rates.

The pair density dependence of the Auger recombination rate per pair at low densities in Fig. 5(a) is n^2, with a coefficient $C=2.9\times10^{-27}$ cm^6/s. At densities near where the valence band becomes degenerate (1.1×10^{18} cm^{-3}), the rate saturates to a linear form. This indicates that the dominant Auger process involves promoting a hole in the valence band rather than an electron in the conduction band. We fit the density dependence with the expression $Cn^2/(1+n/n_{sat})$, where $n_{sat}=3.5\times10^{18}$ cm^{-3}. A fit with saturation is shown by the solid line, while the dashed line shows a fit, without saturation, to the low-density n^2 behavior. The agreement between the theoretical results with umklapp (diamonds) and experimental measurements, *including the saturation behavior*, is remarkable.

We note that to our knowledge this is also the first accurate calculation of the density dependence of the Auger rate

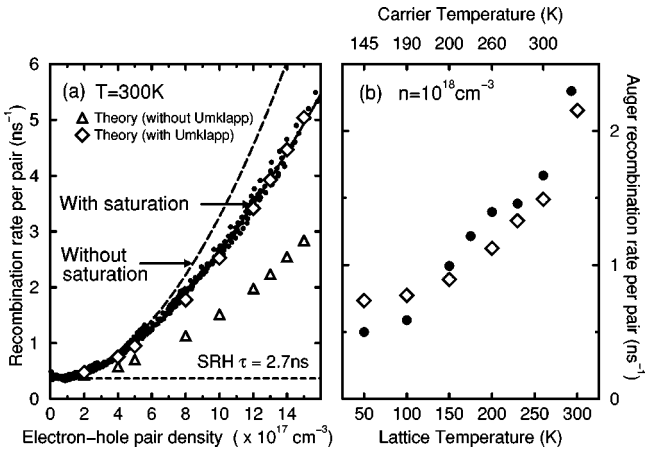

FIG. 5. (a) Theoretical and experimental recombination rate for a 4.0-μm sample at 300 K as a function of the electron-hole pair density determined from differential transmission measurements. The solid line is the fit to the data including saturation to a linear n dependence. The dashed line is the low-density fit without saturation. Results of calculations with (diamonds) and without (triangles) umklapp processes are shown. (b) Rates as a function of temperature determined by PL upconversion (circles) and calculated (diamonds). At temperatures below 300 K the carriers do not cool to the lattice temperature before recombining, so the measured average carrier temperature from 0.01 to 3 ns is also indicated.

in the degenerate regime. Previous calculations either were limited to $T=0$ K (Ref. 1) (predicting a linear rate) or relied on the density-dependence of the rate of the most probable Auger transition (predicting a density-independent Auger rate when both conduction and valence bands are degenerate).[3]

Shown in Fig. 5(b) are Auger rates as a function of temperature for a density of 10^{18} cm^{-3}. An additional difficulty of measurements below room temperature is that the carriers do not cool to the lattice temperature before they recombine.[19]. Hence the Auger calculations are performed with a band structure determined by the lattice temperature and a carrier temperature taken from the high-energy tail of the time-resolved PL spectrum. For this sample the signal to noise of the PL measurements, which require photon counting, is not as good as that of the pump-probe measurements. However, the PL technique provides a straightforward means for accurately measuring the carrier temperature.

An analysis based on the rate of the most probable Auger transition[21] yields an exponential dependence on temperature for nondegenerate semiconductors, $R \propto \exp(\alpha E_g/kT)$, where α depends on electron and hole masses. Both our theoretical and experimental rates increase faster than this expression with temperature. In particular the carrier temperature is the same (300 K) for lattice temperatures of 260 K and 300 K, while the rates (both calculated and measured) are significantly different. The difference is entirely due to subtle changes in the band structure.[20] At a lattice temperature of 260 K most of the hole final states are in the fourth valence subband, whereas at 300 K they are in the third valence subband. This leads to an abrupt increase in the Auger rate between these two lattice temperatures.

VI. CONCLUDING REMARKS

The agreement between theory and experiment for both the 8.8-μm system (77 K) of Ref. 9 and the 4.0-μm system (300 K) measured here is quite remarkable. We note that the Auger calculations performed agree within 25% for both these samples, which were grown by two different researchers in two different machines, and whose Auger rates were measured at different temperatures by two different groups using two very different techniques. The theory-experiment agreement would be impossible without the inclusion of umklapp scattering in the calculations. An additional comment concerning umklapp scattering is that its importance in multiple-quantum-well systems *can exceed an order of magnitude*, due to the smaller value of the reciprocal lattice vector.

Other effects on the electronic structure of the superlattice and the Auger calculations which have been neglected include some many-body effects: screening effects, band-gap renormalization, internal fields, matrix-element enhancement from the Coulomb interaction, and density-dependent broadening of excited states. Due to the large momentum transfer characteristic of the Auger processes, screening is relatively ineffective. We find that calculations including static screening differ from those ignoring screening by about 15% for hole Auger and 5% for electron Auger. Band-gap renormalization, although detectable in the sample at the highest carrier densities, is less than 10 meV. This small effect also suggests that the effects of internal fields (which would primarily act to change the band gap) are small. Matrix-element enhancement at the valence and conduction edges due to the Coulomb attraction of the electron and hole is typically 10% in the dilute limit,[22] and is reduced by screening. Density-dependent broadening is likely overshadowed by broadening due to electron-phonon scattering, which has a characteristic time scale[19] in these structures of ~ 1 ps. Broadening of excited states in general must be less than 10 meV, due to the sharpness of optical features. In contrast, the size of the band-structure feature leading to Auger suppression is roughly 140 meV. Hence this broadening, whatever its source, should not have an important effect on the Auger calculations.

We regard these results as a rigorous test of heterostructure Auger calculations. The measurements presented here show a systematic exploration of the density and temperature dependence of the Auger rate in a type-II heterostructure, and are well reproduced by the calculations, including the transition from n^2 to n behavior. We do note, however, that the linear behavior is apparent in the data from Ref. 9 when it is replotted as in Fig. 3.

ACKNOWLEDGMENTS

This research was supported in part by the United States Air Force, Air Force Materiel Command, Air Force Research Laboratory, Kirtland AFB New Mexico 87117-5777 (Contract F29601-97-C0041), and the National Science Foundation (Grants No. ECS-9406680 and ECS-9707799).

[1] A. Haug, J. Phys. C **16**, 4159 (1983).
[2] A. R. Beattie, J. Phys. C **18**, 6501 (1985).
[3] V. Chazapis, H. A. Blom, K. L. Vodopyanov, A. G. Norman, and C. C. Phillips, Phys. Rev. B **52**, 2516 (1995).
[4] K. L. Vodopyanov, H. Graener, C. C. Phillips, and T. J. Tate, Phys. Rev. B **46**, 13 194 (1992).
[5] B. K. Ridley, *Quantum Processes in Semiconductors* (Clarendon, Oxford, 1988).
[6] A. Sugimura, IEEE J. Quantum Electron. **QE-18**, 352 (1982); N. K. Dutta and R. J. Nelson, J. Appl. Phys. **53**, 74 (1982); L. C. Chiu, P. C. Chen, and A. Yariv, IEEE J. Quantum Electron. **QE-18**, 938 (1982).
[7] M. E. Prise, M. R. Taghizadeh, S. D. Smith, and B. S. Wherrett, Appl. Phys. Lett. **45**, 652 (1984).
[8] Y. Jiang, M. C. Teich, and W. I. Wang, Appl. Phys. Lett. **57**, 2922 (1990); J. Appl. Phys. **69**, 6869 (1991).
[9] E. R. Youngdale, J. R. Meyer, C. A. Hoffman, F. J. Bartoli, C. H. Grein, P. M. Young, H. Ehrenreich, R. H. Miles, and D. H. Chow, Appl. Phys. Lett. **64**, 3160 (1994).
[10] C. H. Grein, P. M. Young, and H. Ehrenreich, Appl. Phys. Lett. **61**, 2905 (1992).
[11] C. H. Grein, P. M. Young, M. E. Flatté, and H. Ehrenreich, J. Appl. Phys. **78**, 7143 (1995).
[12] C. L. Felix, J. R. Meyer, I. Vurgaftman, C.-H. Lin, S. J. Murry, D. Zhang, and S.-S. Pei, IEEE Photonics Technol. Lett. **9**, 734 (1997).
[13] S. Brand and R. A. Abram, J. Phys. C **17**, L571 (1984).
[14] This structure is similar to one proposed as a good candidate for a laser active region by M. E. Flatté, J. T. Olesberg, S. A. Anson, T. F. Boggess, T. C. Hasenberg, R. H. Miles, and C. H. Grein, Appl. Phys. Lett. **70**, 3212 (1997).
[15] M. E. Flatté, P. M. Young, L.-H. Peng, and H. Ehrenreich, Phys. Rev. B **53**, 1963 (1996).
[16] M. E. Flatté, C. H. Grein, H. Ehrenreich, R. H. Miles, and H. Cruz, J. Appl. Phys. **78**, 4552 (1995).
[17] J. T. Olesberg, S. A. Anson, S. W. McCahon, M. E. Flatté, T. F. Boggess, D. H. Chow, and T. C. Hasenberg, Appl. Phys. Lett. **72**, 229 (1998).
[18] S. W. McCahon, S. A. Anson, D.-J. Jang, M. E. Flatté, T. F. Boggess, D. H. Chow, T. C. Hasenberg, and C. H. Grein, Appl. Phys. Lett. **68**, 2135 (1996).
[19] D.-J. Jang, J. T. Olesberg, M. E. Flatté, T. F. Boggess, and T. C. Hasenberg, Appl. Phys. Lett. **70**, 1125 (1997).
[20] D. J. Jang, M. E. Flatté, C. H. Grein, J. T. Olesberg, T. C. Hasenberg, and T. F. Boggess, Phys. Rev. B **58**, 13 047 (1998).
[21] A. R. Beattie and P. T. Landsberg, Proc. R. Soc. London, Ser. A **249**, 16 (1959).
[22] P. M. Young, P. M. Hui, and H. Ehrenreich, Phys. Rev. B **44**, 12 969 (1991).